This article has been accepted for publication in a future issue of this journal, but has not been fully edited. Content may change prior to final publication. Citation information: DOI 10.1109/TPWRD.2020.2995879, IEEE Transactions on Power Delivery

Lagrangian model of an isolated dc-dc converter with a 3-phase medium frequency transformer accounting magnetic cross saturation

Piotr Dworakowski, Andrzej Wilk, *Member, IEEE*, Michal Michna, *Senior Member, IEEE*, Alexis Fouineau, Martin Guillet

***Abstract*—This article presents a nonlinear equivalent circuit model of an isolated dc-dc converter with a 3-phase medium frequency transformer. The model takes into account the magnetic cross saturation of the 3-phase core-type magnetic circuit. The model is suitable in detailed electromagnetic transient simulations of power systems involving isolated dc-dc converters. The model is developed using the Lagrange energy method. It involves a matrix of dynamic inductances containing a nonlinear term resulting from core magnetization and a linear term resulting from leakage flux. The model parameters are determined based on a series of magnetostatic finite element method simulations. This approach is convenient when applied to high power transformers offering a limited characterization effort, or if the transformer prototype does not exist. The experimental validation performed on a novel 3-phase MFT prototype in a 100kW 1.2kV 20kHz dual active bridge converter has proved the validity of the model and model parameters. The no-load steady-state and inrush tests and the full-load test show a very good fit between the simulated and experimentally measured waveforms. The comparison with a classical simplified model neglecting magnetic cross saturation shows a significant difference in the no-load inrush test.**

***Index Terms*— DC-DC power converters, medium frequency transformer, modeling**

I. Introduction

Transformer modelling has been extensively studied for electromagnetic transient simulations of power systems. However, in modern power systems: HVDC grids, smart grids, photovoltaic power plants, wind power plants, and electric vehicle charging, the transformer may be a component of isolated dc-dc power converters [1], [2], [3], [4], [5]. The dual active bridge (DAB) [6] is a promising topology for bidirectional power flow applications. In particular, the 3-phase topology variant is considered for high power applications offering several advantages compared to the single-phase topology [7], [8], [9], [10]. The general circuit diagram of the 3-phase isolated dc-dc converter composed of two voltage source converters (VSC) and a medium frequency transformer (MFT) is shown in Fig. 1. The requirements of the transformer for the 3-phase DAB are different from those for grid connected transformers, considering in particular the operating frequency that can be much higher than 50/60Hz. The modelling requirements differ accordingly.

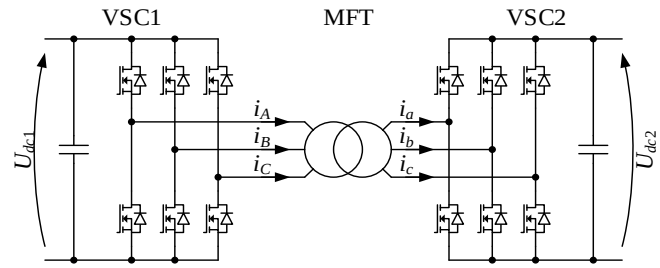

Fig. 1. 3-phase isolated dc-dc converter circuit diagram composed of two voltage source converters (VSC) and a medium frequency transformer (MFT)

The equivalent circuit models can be categorized into distributed and lumped parameter types. The distributed parameter models are used in the analysis of electromagnetic wave propagation based on the transmission line theory. These models are usually used in the analysis of electric devices at high frequency or in the analysis of large power systems. A distributed parameter model of a transformer taking into account the winding capacitances was proposed in [11] and has been further extended in the scientific literature, including [12]. In [13], a distributed parameter model of a buck converter was presented but without providing any clear advantage in power system analysis.

The lumped parameter models simplify the spatially distributed physical system allowing to analyze geometrically complex structures based on discrete elements *R*, *L* and *C*, where the inductance and capacitance may involve self and mutual values. In the most advanced transformer models, a lumped element may correspond to a physical element, for example a winding turn or layer. Detailed lumped parameter transformer models were proposed in [14], [15], [16] and [17]. These models are suitable for high frequency analysis of internal transformer voltages and currents.

The lumped parameter models can also be applied in magnetic core modelling based on magnetic reluctance. The

P. Dworakowski is with SuperGrid Institute, Villeurbanne, France (e-mail: Piotr.DWORAKOWSKI@supergrid-institute.com)

A. Wilk is with the Faculty of Electrical and Control Engineering, Gdansk University of Technology, Gdansk, Poland

M. Michna is with the Faculty of Electrical and Control Engineering, Gdansk University of Technology, Gdansk, Poland

M. Guillet is with SuperGrid Institute, Villeurbanne, France

A. Fouineau is with SuperGrid Institute, Villeurbanne, France

This work is licensed under a Creative Commons Attribution 4.0 License. For more information, see https://creativecommons.org/licenses/by/4.0/.

This article has been accepted for publication in a future issue of this journal, but has not been fully edited. Content may change prior to final publication. Citation information: DOI 10.1109/TPWRD.2020.2995879, IEEE Transactions on Power Delivery

equations of the magnetomotive force (MMF) and the magnetic flux can be transformed to an equivalent electric circuit [18], [19]. The reluctance model can involve a magnetic hysteresis [20]. A hybrid model based on lumped electric and magnetic parameters suitable in electromagnetic transient simulation was proposed in [21] and [22].

In power system analyses, interest is usually focused on transformer's terminal voltages and currents, while neglecting its internal voltages and currents. In [23], [24] and [25], methods were proposed to simplify the detailed models to make them more suitable in power system analyses. In case a detailed model is not available, some measurement techniques can be used to establish the model in time or frequency domain [26], [27], [28], [29], [30], [31].

Many dynamic models of transformer neglect magnetic nonlinearity. The nonlinear 3-phase transformer models are often built from three single-phase transformer models, which makes the analysis of transient states imprecise. The majority of nonlinear 3-phase transformer models neglect the effects of cross couplings between different limbs due to saturation, even if the magnetic cross saturation has been well studied in rotating electrical machines [32], [33]. In [34], a 3-phase 50Hz transformer model including magnetic cross saturation was proposed. The authors of [34] claim that their model is superior when compared to a classical nonlinear model based on three single-phase transformers and neglecting magnetic cross saturation, since it allows to analyze precisely the transformer inrush and fault conditions. In [34], the model parameters were calculated based on measurements performed on a low power transformer.

This article proposes an equivalent circuit model of an isolated dc-dc converter with a 3-phase medium frequency transformer (MFT). According to the state of the art presented above, this model is of a lumped electric parameter type where the transformer model is limited to its terminal voltages and currents. The dc-dc converter model is developed according to the Lagrange energy method described in [35] and [36]. This method was applied for transformer modelling in [37]. In [38] and [39], it was used to model magnetic components of power converters allowing to derive a physically motivated model. The proposed nonlinear MFT model takes into account magnetic cross saturation. The model parameters are calculated based on magnetostatic finite element method (FEM) simulations. Compared to [34], this approach allows to reduce the transformer characterization effort and even to develop a precise model when the transformer prototype is not available. The model parameters are assumed to be constant in the function temperature. The model was validated against the 100kW 1.2kV 20kHz DAB converter reported in [40]. The transformer design is detailed in [41] showing the novelty of the 3-phase structure in medium frequency applications.

The novel aspects of this work include:

- Lagrangian model of 3-phase DAB for electromagnetic transient simulation.
- 3-phase MFT model accounting magnetic cross saturation for precise steady-state and transient analyses.
- Practical approach to the determination of 3-phase MFT model parameters based on magnetostatic FEM simulations.

Derivation of the isolated dc-dc converter model is given in Section II, where the 3-phase MFT magnetic core model is defined with the multi-dimensional flux-MMF characteristic $\mathbf{\Phi}(\mathbf{\Theta})$ and the corresponding derivatives $\partial\mathbf{\Phi}/\partial\mathbf{\Theta}$. Section III presents the approach to the determination of model parameters. A series of magnetostatic FEM simulations have been performed to calculate the required $\mathbf{\Phi}(\mathbf{\Theta})$ based on the known equivalent $B(H)$. In Section IV, the 100kW isolated dc-dc converter test bench is presented, and the model simulation results are compared against the measurement and a classical simplified model.

II. Model derivation

A. Transformer model

Fig. 2 presents the model of the 3-phase core type MFT including the primary windings 1-3 and secondary windings 4-6. Each winding is modelled with the lumped resistance R and the flux linkage $\Psi(\mathbf{i})$. The winding capacitance is neglected since it has a minor effect on the operation of the converter. This will be presented later in this article in the no-load and full-load tests. The core power loss related to hysteresis and eddy current effects is modelled with an equivalent circuit composed of three additional coils 7-9. The system can be described with the equation:

$$\frac{d}{dt}\mathbf{\Psi}(\mathbf{i}) + \mathbf{R}\mathbf{i} = \mathbf{u}(t) \tag{1}$$

where

$$\mathbf{u} = [u_1 \quad u_2 \quad \cdots \quad u_9]^{\mathrm{T}} \tag{2}$$

$$\mathbf{i} = [i_1 \quad i_2 \quad \cdots \quad i_9]^{\mathrm{T}} \tag{3}$$

$$\mathbf{\Psi}(\mathbf{i}) = [\Psi_1(\mathbf{i}) \quad \Psi_2(\mathbf{i}) \quad \cdots \quad \Psi_9(\mathbf{i})]^{\mathrm{T}} \tag{4}$$

$$\mathbf{R} = \mathrm{diag}[R_1 \quad R_2 \quad \cdots \quad R_9] \tag{5}$$

The flux linkage $\Psi(\mathbf{i})$ is a nonlinear function of all transformer currents. The time derivative of the flux linkage vector $\mathbf{\Psi}(\mathbf{i}(t))$ defines the electromotive force in each winding and can be expressed as the matrix of dynamic inductances $\mathbf{L_d}$:

$$\frac{d}{dt}\mathbf{\Psi}\big(\mathbf{i}(t)\big) = \begin{bmatrix} \frac{\partial\Psi_1}{\partial i_1} & \cdots & \frac{\partial\Psi_1}{\partial i_9} \\ \vdots & & \vdots \\ \frac{\partial\Psi_9}{\partial i_1} & \cdots & \frac{\partial\Psi_9}{\partial i_9} \end{bmatrix} \frac{d}{dt}\begin{bmatrix} i_1 \\ \vdots \\ i_9 \end{bmatrix} = \mathbf{L_d}(\mathbf{i})\frac{d}{dt}\mathbf{i} \tag{6}$$

According to [42] and [43], it can be assumed that the matrix of dynamic inductances $\mathbf{L_d}$ contains a nonlinear term resulting from core magnetization and a linear term resulting from flux leakage. The flux linkage can be represented as follows:

$$\Psi_k(\mathbf{i}) = N_k\Phi_k\big(\mathbf{\Theta}(\mathbf{i})\big) + \sum_{n=1}^{9} L_{\sigma k,n} i_n \tag{7}$$

where k=1, 2, ..., 9 is the winding index, N is the number of turns, and

$$\mathbf{\Theta} = [i_1N_1 \quad i_2N_2 \quad \cdots \quad i_9N_9]^{\mathrm{T}} \tag{8}$$

MOST WIEDZY Downloaded from mostwiedzy.pl

This work is licensed under a Creative Commons Attribution 4.0 License. For more information, see https://creativecommons.org/licenses/by/4.0/.

This article has been accepted for publication in a future issue of this journal, but has not been fully edited. Content may change prior to final publication. Citation information: DOI 10.1109/TPWRD.2020.2995879, IEEE Transactions on Power Delivery

A further assumption is made that there is a magnetizing flux $\mathbf{\Phi_m}$ which is coupled with all windings:

$$\mathbf{\Phi_m} = \begin{bmatrix} \Phi_{m1}(\mathbf{\Theta_m}) \\ \Phi_{m2}(\mathbf{\Theta_m}) \\ \Phi_{m3}(\mathbf{\Theta_m}) \end{bmatrix} \tag{9}$$

where $\mathbf{\Theta_m}$ is the magnetizing MMF defined as:

$$\mathbf{\Theta_m} = \begin{bmatrix} i_1N_1 + i_4N_4 + i_7N_7 \\ i_2N_2 + i_5N_5 + i_8N_8 \\ i_3N_3 + i_6N_6 + i_9N_9 \end{bmatrix} \tag{10}$$

Finally, the matrix of dynamic inductances $\mathbf{L_d}$ is:

$$\mathbf{L_d} = \begin{bmatrix} N_1\frac{\partial\Phi_{m1}}{\partial\Theta_{m1}}N_1 & N_1\frac{\partial\Phi_{m1}}{\partial\Theta_{m2}}N_2 & \dots & N_1\frac{\partial\Phi_{m1}}{\partial\Theta_{m3}}N_9 \\ N_2\frac{\partial\Phi_{m2}}{\partial\Theta_{m1}}N_1 & N_2\frac{\partial\Phi_{m2}}{\partial\Theta_{m2}}N_2 & \dots & N_2\frac{\partial\Phi_{m2}}{\partial\Theta_{m3}}N_9 \\ \vdots & \vdots & & \vdots \\ N_9\frac{\partial\Phi_{m3}}{\partial\Theta_{m1}}N_1 & N_9\frac{\partial\Phi_{m3}}{\partial\Theta_{m2}}N_2 & \dots & N_9\frac{\partial\Phi_{m3}}{\partial\Theta_{m3}}N_9 \end{bmatrix} + \begin{bmatrix} L_{\sigma1,1} & L_{\sigma1,2} & \dots & L_{\sigma1,9} \\ L_{\sigma2,1} & L_{\sigma2,2} & \dots & L_{\sigma2,9} \\ \vdots & \vdots & & \vdots \\ L_{\sigma9,1} & L_{\sigma9,2} & \dots & L_{\sigma9,9} \end{bmatrix} \tag{11}$$

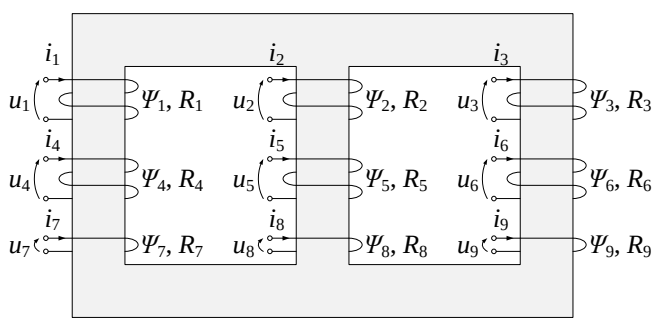

Fig. 2. Model of a 3-phase MFT with primary winding 1-3, secondary winding 4-6, and equivalent circuit 7-9 for core power loss

B. Equivalent circuit model of isolated dc-dc converter

The equivalent circuit model of an isolated dc-dc converter is presented in Fig. 3. In this model, each voltage source converter (VSC) is modelled with three controlled voltage sources with U_{dc1} or U_{dc2} input. The MFT is connected in Yy vector group. The equivalent circuit for core power loss is included in the model with the resistances R_7, R_8 and R_9. In order to facilitate the further analysis, these resistances are star-connected. Finally, the loop currents i_{g1}, i_{g2}, ..., i_{g6} are defined.

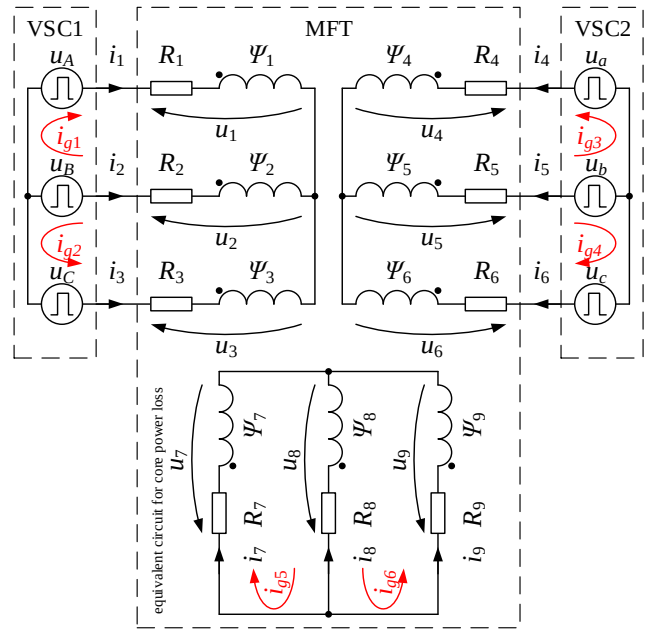

Fig. 3. Equivalent circuit model of a 3-phase DAB converter including the Yy connected MFT with equivalent circuit for core power loss

C. Lagrange energy method

The transformer model is further developed according to the Lagrange energy method. The Lagrange function and the Rayleigh dissipation function [35], [36] in nongeneralized coordinates are defined as (considering the linear resistance):

$$\mathcal{L}(\mathbf{i}) = \sum_{k=1}^{9}\int_0^{i_k}\Psi_k(\mathbf{i})\,di_k \tag{12}$$

$$P_e(\mathbf{i}) = \frac{1}{2}\sum_{k=1}^{9}R_k{i_k}^2 \tag{13}$$

The equation of constraints is defined according to Fig. 3 as:

$$\mathbf{i} = \begin{bmatrix} 1 & 0 & 0 & 0 & 0 & 0 \\ -1 & -1 & 0 & 0 & 0 & 0 \\ 0 & 1 & 0 & 0 & 0 & 0 \\ 0 & 0 & 1 & 0 & 0 & 0 \\ 0 & 0 & -1 & -1 & 0 & 0 \\ 0 & 0 & 0 & 1 & 0 & 0 \\ 0 & 0 & 0 & 0 & 1 & 0 \\ 0 & 0 & 0 & 0 & -1 & -1 \\ 0 & 0 & 0 & 0 & 0 & 1 \end{bmatrix}\mathbf{i_g} \tag{14}$$

where

$$\mathbf{i_g} = [i_{g1} \quad i_{g2} \quad \cdots \quad i_{g6}]^{\mathrm{T}} \tag{15}$$

Equation (14) is inserted into (12) and (13) to obtain the Lagrange function and the Rayleigh dissipation function in generalized coordinates.

The general form of the Euler-Lagrange equation system is:

$$\frac{d}{dt}\frac{\partial\mathcal{L}(\mathbf{i_g})}{\partial i_{gk}} + \frac{\partial P_e(\mathbf{i_g})}{\partial i_{gk}} = Q_k \tag{16}$$

where k=1, 2, ..., 6, and Q_k is the generalized force defined as:

$$\mathbf{Q} = [u_A - u_B \quad u_C - u_B \quad u_a - u_b \quad u_c - u_b \quad 0 \quad 0]^{\mathrm{T}} \tag{17}$$

The final matrix form of the Euler-Lagrange equation is:

MOST WIEDZY Downloaded from mostwiedzy.pl

This work is licensed under a Creative Commons Attribution 4.0 License. For more information, see https://creativecommons.org/licenses/by/4.0/.

This article has been accepted for publication in a future issue of this journal, but has not been fully edited. Content may change prior to final publication. Citation information: DOI 10.1109/TPWRD.2020.2995879, IEEE Transactions on Power Delivery

$$\mathbf{M_s}(\mathbf{i_g})\frac{d}{dt}\mathbf{i_g} + \mathbf{R_s}\mathbf{i_g} = \mathbf{Q} \tag{18}$$

where:

$$\mathbf{R_s} = \begin{bmatrix} R_1 + R_2 & R_2 & \cdots & 0 \\ R_2 & R_2 + R_3 & \cdots & 0 \\ \vdots & \vdots & & \vdots \\ 0 & 0 & \cdots & R_8 + R_9 \end{bmatrix} \tag{19}$$

$$\mathbf{M_s} = \begin{bmatrix} \frac{\partial \Psi_1}{\partial i_{g1}} - \frac{\partial \Psi_2}{\partial i_{g1}} & \frac{\partial \Psi_1}{\partial i_{g2}} - \frac{\partial \Psi_2}{\partial i_{g2}} & \cdots & \frac{\partial \Psi_1}{\partial i_{g6}} - \frac{\partial \Psi_2}{\partial i_{g6}} \\ \frac{\partial \Psi_3}{\partial i_{g1}} - \frac{\partial \Psi_2}{\partial i_{g1}} & \frac{\partial \Psi_3}{\partial i_{g2}} - \frac{\partial \Psi_2}{\partial i_{g2}} & \cdots & \frac{\partial \Psi_3}{\partial i_{g6}} - \frac{\partial \Psi_2}{\partial i_{g6}} \\ \vdots & \vdots & & \vdots \\ \frac{\partial \Psi_9}{\partial i_{g1}} - \frac{\partial \Psi_8}{\partial i_{g1}} & \frac{\partial \Psi_9}{\partial i_{g2}} - \frac{\partial \Psi_8}{\partial i_{g2}} & \cdots & \frac{\partial \Psi_9}{\partial i_{g6}} - \frac{\partial \Psi_8}{\partial i_{g6}} \end{bmatrix} \tag{20}$$

According to Section II-A, the matrix $\mathbf{M_s}$ can be split into nonlinear and linear terms, which gives:

$$\mathbf{M_s} = \begin{bmatrix} N_p \frac{\partial \Phi_{m1}}{\partial \Theta_{g1}} N_p - N_p \frac{\partial \Phi_{m2}}{\partial \Theta_{g1}} N_p & \cdots & N_p \frac{\partial \Phi_{m1}}{\partial \Theta_{g2}} N_e - N_p \frac{\partial \Phi_{m2}}{\partial \Theta_{g2}} N_e \\ \vdots & & \vdots \\ N_e \frac{\partial \Phi_{m3}}{\partial \Theta_{g1}} N_p - N_e \frac{\partial \Phi_{m2}}{\partial \Theta_{g1}} N_p & \cdots & N_e \frac{\partial \Phi_{m3}}{\partial \Theta_{g2}} N_e - N_e \frac{\partial \Phi_{m2}}{\partial \Theta_{g2}} N_e \end{bmatrix} + \begin{bmatrix} L_{\sigma 1,1} - L_{\sigma 2,1} & \cdots & 0 \\ \vdots & & \vdots \\ 0 & \cdots & 0 \end{bmatrix} \tag{21}$$

where $\mathbf{\Theta_g}$ is the magnetizing MMF in generalized coordinates:

$$\mathbf{\Theta_g} = \begin{bmatrix} i_{g1}N_p + i_{g3}N_s + i_{g5}N_e \\ i_{g2}N_p + i_{g4}N_s + i_{g6}N_e \end{bmatrix} \tag{22}$$

and N_p is the number of primary turns, N_s is the number of secondary turns, N_e is the number of turns in the equivalent core loss coil. The leakage inductances of the equivalent circuit for core power loss are assumed to be equal to zero.

It is noted that for the Yy transformer, the magnetizing flux $\mathbf{\Phi_m}$ is simplified to:

$$\mathbf{\Phi_m} = \begin{bmatrix} \Phi_{m1}(\mathbf{\Theta_g}) \\ \Phi_{m2}(\mathbf{\Theta_g}) \\ \Phi_{m3}(\mathbf{\Theta_g}) \end{bmatrix} \tag{23}$$

being a function of 2 variables. Consequently, it can be easily analyzed and visualized.

The model can be implemented in any computational software. The authors have implemented it in a Matlab script.

III. Model Parameters

A. Approach

The major difficulty in transformer modelling consists in parameter determination. In [34], a significant number of measurements were performed on the existing low power transformer. However, this approach can be challenging when applied to high power transformers. That is why an alternative approach is proposed in this article. It is based on the known equivalent $B(H)$ and a simplified FEM simulation model using homogenized winding and core materials. The equivalent $B(H)$ can be measured using the approach proposed in [44]. In case the modelled transformer does not exist, the $B(H)$ scaling function proposed in [45] for ferrite core MFT can be used.

B. Finite element model

A simplified 3D MFT model was developed in Ansys Maxwell. The model was divided into three computational domains. The domain Ω_1 is the volume of the windings, the domain Ω_2 is the volume of the core, and the domain Ω_3 consists of the air surrounding the MFT. The material properties have been considered isotropic and homogenized, so the Maxwell's equations can be simplified to:

$$\nabla \times \boldsymbol{H} = \begin{cases} \boldsymbol{j} & \text{in } \Omega_1 \\ \sigma \boldsymbol{E} & \text{in } \Omega_2 \\ 0 & \text{in } \Omega_3 \end{cases} \tag{24}$$

$$\nabla \times \boldsymbol{E} = -\frac{\partial \boldsymbol{B}}{\partial t}; \quad \nabla \bullet \boldsymbol{B} = 0; \quad \boldsymbol{B} = \nabla \times \boldsymbol{A} \tag{25}$$

where σ = 0.25S/m at 25˚C. The equivalent anhysteretic $B(H)$, measured by the authors in [45], is presented in Fig. 4. The ferrite 3C90 $B(H)$ from datasheet [46] is also presented for comparison. Significant difference between the two curves is due to multiple parasitic air gaps which are the result of core assembly from I-type cores. Moreover, due to manufacturing tolerances, the I-core is not an ideal rectangular cuboid and its dimensions vary from one sample to another. This causes the non-uniform parasitic air gaps in the core which are unpredictable at the industrial design stage and which cannot be modelled precisely. In [45], it is presented that the relative average air gap length is nonlinearly increasing with the number of air gaps due to the cumulating I-core misalignments. In the 3-phase MFT, the average air gap length is approximately 0.7mm, out of the 1m magnetic circuit length.

The ferrite $B(H)$ is also a function of temperature what can be observed in the 3C90 datasheet [46]. In particular, the maximum flux density, magnetic permeability and power loss are lower at 100˚C than at 25˚C. However, the influence of temperature is not analyzed in this article. The authors consider that the equivalent anhysteretic $B(H)$ is mainly influenced by the parasitic air gaps. The temperature has a major influence on the core power loss but the power loss is not the focus of this article.

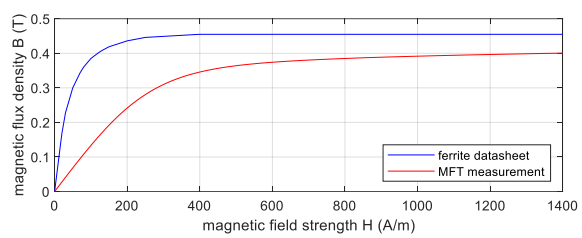

Fig. 4. Equivalent anhysteretic $B(H)$ from ferrite 3C90 datasheet at 25°C (blue) and MFT measurement at 25°C (red)

C. Magnetostatic simulation

To calculate the $\mathbf{\Phi(\Theta)}$ multi-dimensional characteristic required for the circuit model, a series of magnetostatic simulations are to be performed with different MMFs. Considering the Yy vector group, the set of simulations can be reduced since the sum of primary or secondary MMFs is equal

MOST WIEDZY Downloaded from mostwiedzy.pl

This work is licensed under a Creative Commons Attribution 4.0 License. For more information, see https://creativecommons.org/licenses/by/4.0/.

This article has been accepted for publication in a future issue of this journal, but has not been fully edited. Content may change prior to final publication. Citation information: DOI 10.1109/TPWRD.2020.2995879, IEEE Transactions on Power Delivery

to zero. Practically, the authors define the primary and secondary excitations as:

$$\mathbf{\Theta_p} = [\Theta_1 \quad \Theta_2 \quad \Theta_3] \tag{26}$$

$$\mathbf{\Theta_s} = [\Theta_4 \quad \Theta_5 \quad \Theta_6] \tag{27}$$

where Θ_1, Θ_3, Θ_4 and Θ_6 have discrete values in the range [-20e3, 20e3] A, and

$$\Theta_2 = -\Theta_1 - \Theta_3 \tag{28}$$

$$\Theta_5 = -\Theta_4 - \Theta_6 \tag{29}$$

The magnetizing flux of side columns Φ_{m1} and Φ_{m3} was measured in the yoke in order to minimize the leakage flux contribution. The magnetizing flux of the central column was calculated with:

$$\Phi_{m2} = -\Phi_{m1} - \Phi_{m3} \tag{30}$$

The series of magnetostatic simulations requires approximately one working day using a coarse mesh and a standard workstation.

D. Magnetizing flux

Fig. 5 presents the result of the series of magnetostatic simulations for column 1 and the corresponding surface interpolation. The effect of magnetic cross saturation can be observed as the shape of the curve $\Phi_{m1}(\Theta_{g1})$ (equivalent to $B(H)$) is depending on the value of Θ_{g2}. The maximum value of the magnetizing flux is 0.55mWb, which corresponds to the magnetic flux density of 0.44T.

Thanks to the magnetizing flux $\mathbf{\Phi_m}$ surface interpolation, the partial derivatives $\partial\mathbf{\Phi_m}/\partial\mathbf{\Theta_g}$ can be easily calculated. The partial derivatives for column 1 are presented in Fig. 6 and Fig. 7. The values of $\partial\Phi_{m1}/\partial\Theta_{g1}$ are always positive, with the maximum value of 4.6μWb/A corresponding to the self-magnetizing inductance for generalized loop currents of 1.8mH. The maximum value of $\partial\Phi_{m1}/\partial\Theta_{g2}$ is 1.5μWb/A and it corresponds to the mutual magnetizing inductance for generalized loop currents of 0.6mH. The partial derivative functions are directly used in the model to calculate the values of the dynamic inductance matrix.

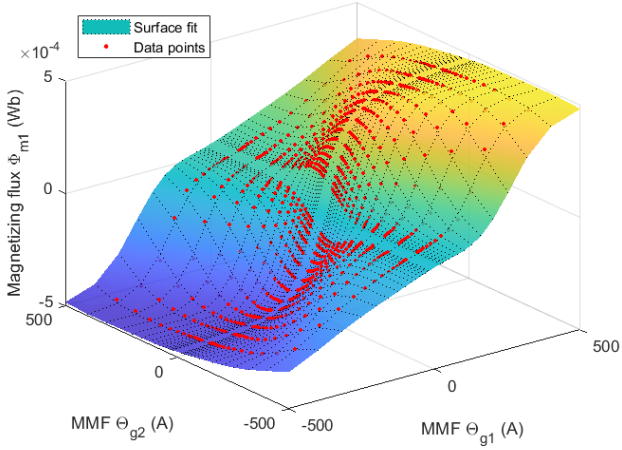

Fig. 5. Magnetizing flux Φ_{m1} as function of magnetizing MMF in generalized coordinates Θ_{g1} and Θ_{g2}

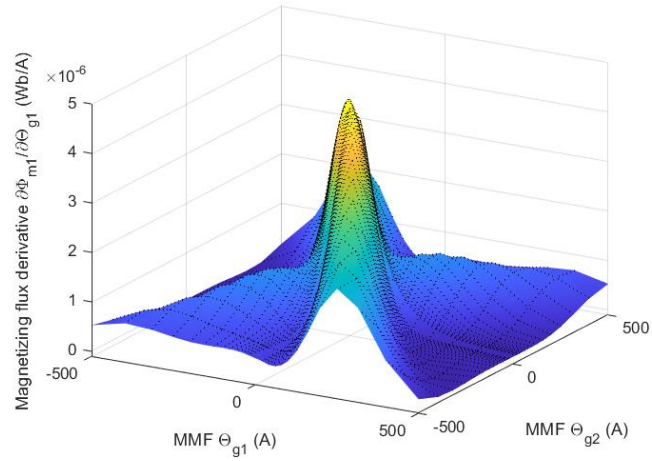

Fig. 6. Magnetizing flux partial derivative $\partial\Phi_{m1}/\partial\Theta_{g1}$ as function of magnetizing MMF in generalized coordinates Θ_{a1} and Θ_{a2}

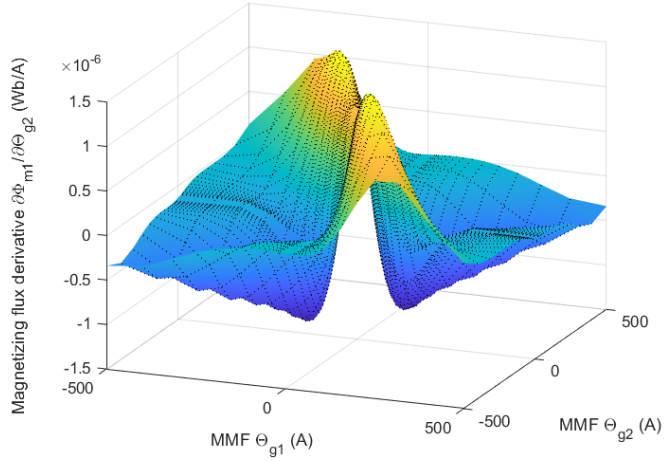

Fig. 7. Magnetic flux partial derivative $\partial\Phi_{m1}/\partial\Theta_{g2}$ as function of magnetizing MMF in generalized coordinates Θ_{g1} and Θ_{g2}

E. Leakage inductance and resistance

The leakage inductance matrix is calculated according to (7), where the flux linkage comes directly from the magnetostatic simulation. The number of primary N_p and secondary N_s turns is equal to 20. The equivalent leakage inductance values for generalized loop currents are presented in Table I. It can be observed that the mutual leakage inductances ([42], [43]) have significant values, as a result of magnetic flux coupling through the air.

TABLE I
EQUIVALENT LEAKAGE INDUCTANCE MATRIX FOR GENERALIZED LOOP CURRENTS (μH)

$L_{\sigma k,n}$	n=1	n=2	n=3	n=4
k=1	56.1	-2.9	48.2	-2.4
k=2	-9.4	-9.4	2.0	2.0
k=3	-2.9	56.1	-2.5	48.2
k=4	48.2	-2.5	56.1	-2.1
k=5	-11.4	-11.4	-15.5	-15.5
k=6	-2.4	48.2	-2.1	56.1

The MFT winding resistance is difficult to calculate due to skin and proximity effects. The analytical formula for round litz wire was proposed in [47] based on [48]. The authors presented the winding resistance calculation in [41] and a good fit was observed between the calculation and a measurement with an impedance analyzer. In addition, the connection wire resistance

MOST WIEDZY Downloaded from mostwiedzy.pl

This work is licensed under a Creative Commons Attribution 4.0 License. For more information, see https://creativecommons.org/licenses/by/4.0/.

This article has been accepted for publication in a future issue of this journal, but has not been fully edited. Content may change prior to final publication. Citation information: DOI 10.1109/TPWRD.2020.2995879, IEEE Transactions on Power Delivery

between the VSC and the transformer terminals, and the VSC power semiconductor switch on-state resistance and switching loss have to be taken into account. According to [49], the MOSFET on-state resistance varies from 8mΩ at 25°C and 16mΩ at 150°C. The model resistance values are calculated as a sum of the above mentioned components and presented in Table II. The resistance of the equivalent circuit for core power loss takes into account the hysteresis and eddy current power loss. The analytical formula for core power loss with non-sinusoidal excitations was proposed in [50] based on [51]. The resistance value of the equivalent circuit for core power loss is calculated at the nominal voltage and presented in Table II. The number of turns N_e for this equivalent circuit was chosen to be equal to 1.

TABLE II
RESISTANCES OF THE DAB EQUIVALENT CIRCUIT MODEL AT 20KHZ (Ω)

primary resistance R_1, R_2, R_3	0.020
secondary resistance R_4, R_5, R_6	0.024
equivalent core loss resistance R_7, R_8, R_9	5

The winding parasitic capacitances are not taken into account in the model because they have very low values, in the range of tens of pF.

IV. EXPERIMENTAL VERIFICATION

A. Converter test bench

The 100kW dc-dc power converter test bench is shown in Fig. 8 with VSC1, VSC2, and the 3-phase MFT prototype. Three test types were considered to validate the proposed model: the MFT no-load steady-state test, the MFT no-load inrush test, and the DAB full-load test. All tests were performed at the ambient temperature of 25°C. The measured MFT temperature was nearly equal to the ambient temperature, as the tests lasted for few minutes only. The VSC operates in the rectangular modulation where each leg is switched at 20kHz with 50% duty cycle and the only controlled variable is the phase shift between two VSCs. The duty cycle may be adjusted in a very small range to control the transformer DC bias.

In the MFT no-load tests, the VSC1 was supplied from a DC power supply, and the AC terminals of the VSC2 were disconnected. The VSC1 was launched normally with 1200Vdc input voltage. In the inrush test the MFT current was captured just after the VSC1 launch, while in the steady-state test it was captured after few seconds.

In the DAB full-load test, the power circuit was arranged in back-to-back configuration, in order to test the dc-dc converter with minimum power consumption. The converter output was connected to its input and the whole was supplied from the DC power supply which set the voltage reference and supplied the test circuit power loss. The dc-dc converter operated in the power regulation mode at 100kW and the steady-state waveforms were recorded.

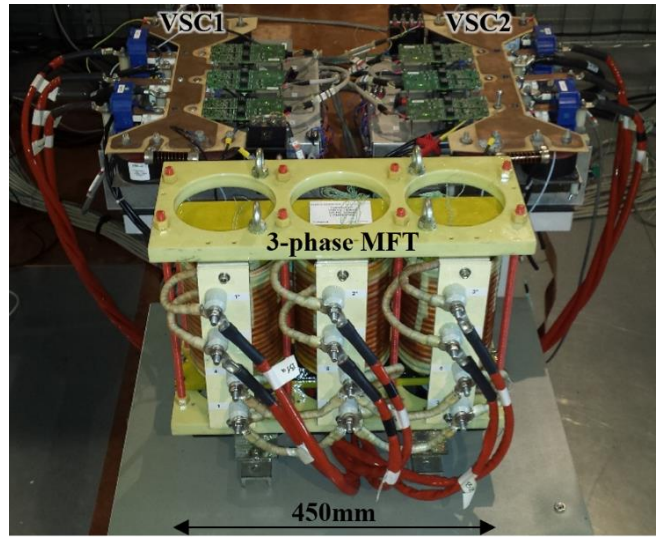

Fig. 8. 100kW 3-phase isolated dc-dc converter test bench

B. MFT no-load test - steady state

In Fig. 9 and Fig. 10, the simulation result is compared against the MFT no-load steady-state test measurement. The voltage waveforms show good synchronization between the simulation and the measurement. The measured magnetizing current is compared against two simulation models: a classical simplified model neglecting magnetic cross saturation, and the complete model including the cross saturation. In reference to the cross saturation model characterized by (23), the simplified model is characterized by:

$$\mathbf{\Phi_m} = \begin{bmatrix} \Phi_{m1}(\Theta_{g1}) \\ -\Phi_{m1}(\Theta_{g1}) - \Phi_{m3}(\Theta_{g2}) \\ \Phi_{m3}(\Theta_{g2}) \end{bmatrix} \tag{31}$$

The cross saturation model shows quite a good fit to the measurement. Small differences are due to the dissymmetry between the three columns. The classical simplified model fits a bit less, but it also gives acceptable results. It can be seen that neglecting winding capacitances was a fair assumption. There are some current oscillations in the measured current but they are low.

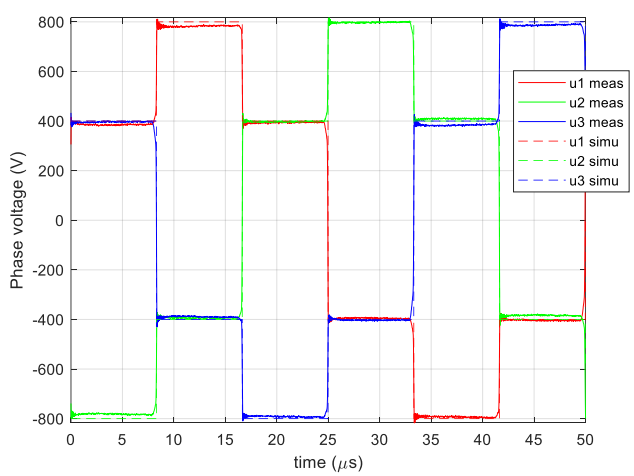

Fig. 9. MFT no-load steady-state test - comparison of transformer phase voltage waveforms: simulation model (dashed line) and measurement (solid line)

MOST WIEDZY Downloaded from mostwiedzy.pl

This work is licensed under a Creative Commons Attribution 4.0 License. For more information, see https://creativecommons.org/licenses/by/4.0/.

This article has been accepted for publication in a future issue of this journal, but has not been fully edited. Content may change prior to final publication. Citation information: DOI 10.1109/TPWRD.2020.2995879, IEEE Transactions on Power Delivery

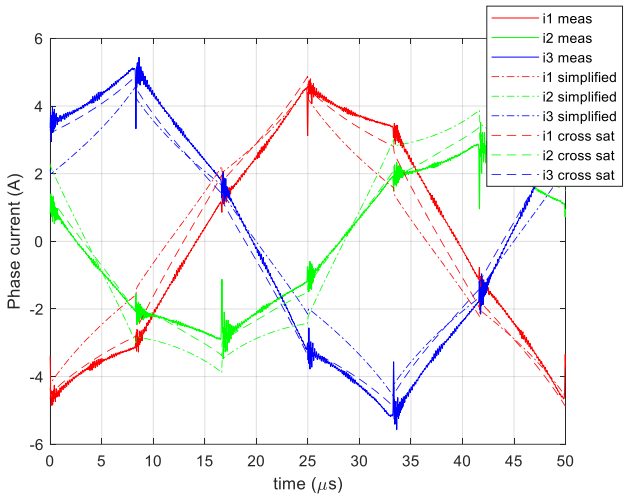

Fig. 10. MFT no-load steady-state test - comparison of magnetizing current waveforms: simplified model (dash-dotted line), cross saturation model (dashed line) and measurement (solid line)

C. *MFT no-load test - inrush*

In Fig. 11, the classical simplified model simulation result is compared against the MFT no-load inrush test measurement. Very significant differences are observed.

In Fig. 12, the proposed cross saturation model simulation result is compared against the measurement, and a very good fit is observed in the magnetizing current. This proves the accuracy of the proposed model and method for model parameter calculation. In particular, this test confirms the validity of the multi-dimensional characteristic of magnetizing flux $\mathbf{\Phi}(\mathbf{\Theta})$ (Fig. 5).

In Fig. 13, the magnetizing current is displayed on the surface plot of the magnetizing flux Φ_{m3} as the function of the magnetizing MMF. This allows to observe the effect of magnetic cross saturation. Indeed, the saturation of winding 3 is influenced by the value of the current in winding 1 (and winding 2, due to the Yy connection).

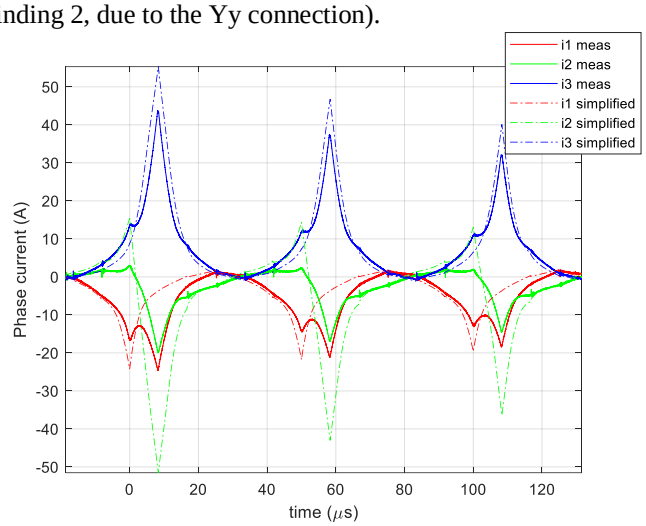

Fig. 11. MFT no-load inrush test - comparison of magnetizing current waveforms: simplified model (dash-dotted line) and measurement (solid line)

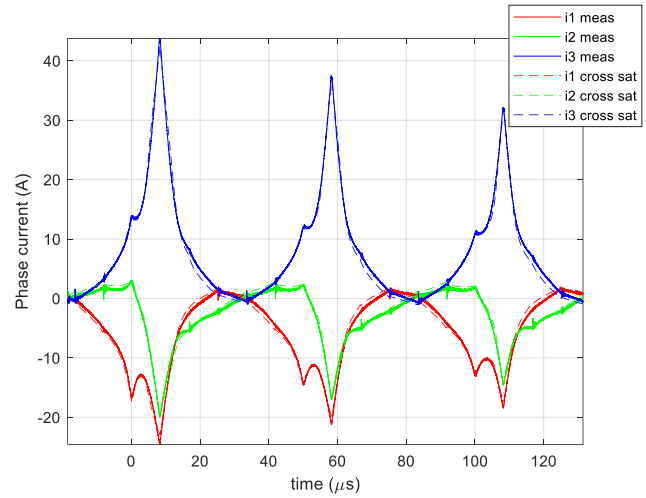

Fig. 12. MFT no-load inrush test - comparison of magnetizing current waveforms: cross saturation model (dashed line) and measurement (solid line)

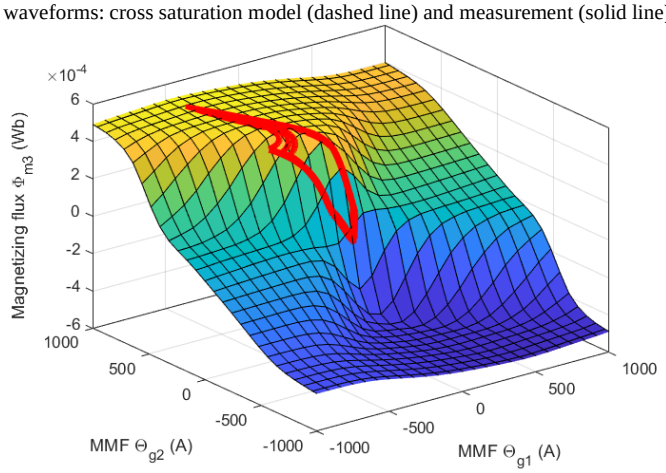

Fig. 13. MFT no-load inrush test - visualization of the magnetizing current from Fig. 12 on the surface of magnetizing flux Φ_{m3} as function of the magnetizing MMF in generalized coordinates Θ_{g1} and Θ_{g2}

D. *DAB full load test*

Fig. 14 compares the cross saturation model simulation result against the DAB full-load test steady-state measurement. A good fit is observed in the phase shift between the primary and secondary voltage, and as the consequence in the current waveform. A very small difference is probably due to the fact that the inductance of connection wires is neglected in the model. The connection wire is approximately 3 meters so it adds a few microhenries to the 16μH leakage inductance. The simplified model gives a very similar result. This test proves in particular the validity of the leakage inductance matrix (Table I).

MOST WIEDZY Downloaded from mostwiedzy.pl

This work is licensed under a Creative Commons Attribution 4.0 License. For more information, see https://creativecommons.org/licenses/by/4.0/.

This article has been accepted for publication in a future issue of this journal, but has not been fully edited. Content may change prior to final publication. Citation information: DOI 10.1109/TPWRD.2020.2995879, IEEE Transactions on Power Delivery

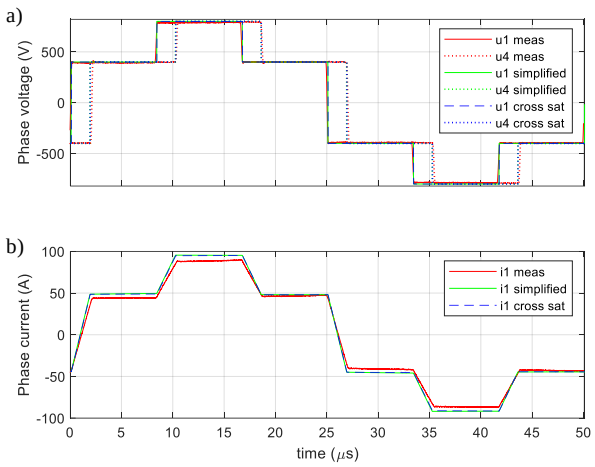

Fig. 14. DAB full-load test - comparison of voltage (a) and current (b) waveforms: simplified model (green), cross saturation model (blue) and measurement (red)

V. Conclusions

The equivalent circuit model of the 3-phase dual active bridge converter is presented. The model has been developed using the Lagrange energy method. The nonlinear transformer model takes into account the magnetic cross saturation of the 3-phase core-type magnetic circuit without developing a reluctance model. It involves a matrix of dynamic inductances containing a nonlinear term resulting from core magnetization and a linear term resulting from leakage flux. The model parameters were determined based on a series of magnetostatic FEM simulations. This approach is convenient when applied to high power transformers, or when the transformer prototype does not exist.

The experimental validation performed on a novel 3-phase MFT prototype in a 100kW 1.2kV 20kHz DAB converter has proved the validity of the model and model parameters. The no-load steady-state and inrush tests, and the full-load test show a very good fit between the waveforms obtained from simulation and measurement. The comparison with a classical simplified model neglecting magnetic cross saturation reveals a very significant difference in the inrush test.

The proposed model can be used in electromagnetic transient simulations of modern power systems, where the 3-phase transformer is part of an isolated dc-dc converter. The simulation time of few fundamental periods on a standard PC varies from few seconds to 1 hour depending on the solver precision, degree of nonlinearity and VSC voltage waveform shape (sinusoidal or square).

The model should be further developed taking into account the temperature effect on winding and core. The transformer model can be improved taking into account an advanced model of magnetic hysteresis. This would allow a precise calculation of core power loss. The VSC model can be improved taking into account the SiC MOSFET behavior. The model can also be easily extended with parasitic winding capacitance, in cases when the capacitance has a significant value.

Acknowledgment

This work was supported by a grant overseen by the French National Research Agency (ANR) as part of the “Investissements d’Avenir” Program (ANE-ITE-002-01) and the LINTE^2 Laboratory at the Gdansk University of Technology (Poland).

References

[1] D. Gómez A. et al., "Requirements for interconnection of HVDC links with DC-DC converters," IECON 2019 - 45th Annual Conference of the IEEE Industrial Electronics Society, Lisbon, Portugal, 2019, pp. 4854-4860

[2] M. Adamowicz, "Power Electronics Building Blocks for implementing Smart MV/LV Distribution Transformers for Smart Grid," Acta Energetica, vol. 4, no. 21, pp. 6-13, Oct. 2014

[3] G. R. Walker and P. C. Sernia, "Cascaded DC-DC converter connection of photovoltaic modules," IEEE Transactions on Power Electronics, vol. 19, no. 4, pp. 1130–1139, Jul. 2004

[4] C. G. Dincan et al., "Design of a High-Power Resonant Converter for DC Wind Turbines," in IEEE Transactions on Power Electronics, vol. 34, no. 7, pp. 6136-6154, July 2019

[5] Y. Du, S. Lukic, B. Jacobson, and A. Huang, "Review of high power isolated bi-directional DC-DC converters for PHEV/EV DC charging infrastructure," 2011 IEEE Energy Conversion Congress and Exposition, pp. 553–560, 2011

[6] R. W. A. A. De Doncker, D. M. Divan and M. H. Kheraluwala, "A three-phase soft-switched high-power-density DC/DC converter for high-power applications," in IEEE Transactions on Industry Applications, vol. 27, no. 1, pp. 63-73, Jan.-Feb. 1991

[7] A. R. Prasad, P. D. Ziogas and S. Manias, "Analysis and design of a three-phase offline DC-DC converter with high-frequency isolation," in IEEE Transactions on Industry Applications, vol. 28, no. 4, pp. 824-832, July-Aug. 1992

[8] N. Soltau, H. Stagge, R. W. De Doncker and O. Apeldoorn, "Development and demonstration of a medium-voltage high-power DC-DC converter for DC distribution systems," 2014 IEEE 5th International Symposium on Power Electronics for Distributed Generation Systems (PEDG), Galway, 2014, pp. 1-8

[9] J. Xue, F. Wang, D. Boroyevich and Z. Shen, "Single-phase vs. three-phase high density power transformers," 2010 IEEE Energy Conversion Congress and Exposition, Atlanta, GA, 2010, pp. 4368-4375

[10] M. Noah et al., "A novel three-phase LLC resonant converter with integrated magnetics for lower turn-off losses and higher power density," 2017 IEEE Applied Power Electronics Conference and Exposition (APEC), Tampa, FL, 2017, pp. 322-329

[11] R. Rudenberg, "Performance of traveling waves in coils and windings," in Electrical Engineering, vol. 59, no. 12, pp. 1031-1040, Dec. 1940

[12] F. Della Torre, A. P. Morando and G. Todeschini, "Three-Phase Distributed Model of High-Voltage Windings to Study Internal Steep-Fronted Surge Propagation in a Straightforward Transformer," in IEEE Transactions on Power Delivery, vol. 23, no. 4, pp. 2050-2057, Oct. 2008

[13] C. Huang, F. Woittennek, and K. Röbenack, “Distributed parameter model of the buck converter with constant inductive load,” IFAC-PapersOnLine, vol. 48, no. 1, pp. 691–692, Jan. 2015

[14] T. J. Lewis, "The transient behaviour of ladder networks of the type representing transformer and machine windings," in Proceedings of the IEE - Part II: Power Engineering, vol. 101, no. 83, pp. 541-553, October 1954

[15] P. I. Fergestad and T. Henriksen, "Transient Oscillations in Multiwinding Transformers," in IEEE Transactions on Power Apparatus and Systems, vol. PAS-93, no. 2, pp. 500-509, March 1974

[16] R. C. Degeneff, "A general method for determining resonances in transformer windings," in IEEE Transactions on Power Apparatus and Systems, vol. 96, no. 2, pp. 423-430, March 1977

[17] Y. Shibuya and S. Fujita, "High frequency model and transient response of transformer windings," IEEE/PES Transmission and Distribution Conference and Exhibition, Yokohama, Japan, 2002, pp. 1839-1844 vol.3

[18] G. R. Slemon, "Equivalent circuits for transformers and machines including non-linear effects," in Proceedings of the IEE - Part IV: Institution Monographs, vol. 100, no. 5, pp. 129-143, October 1953

MOST WIEDZY Downloaded from mostwiedzy.pl

This work is licensed under a Creative Commons Attribution 4.0 License. For more information, see https://creativecommons.org/licenses/by/4.0/.

This article has been accepted for publication in a future issue of this journal, but has not been fully edited. Content may change prior to final publication. Citation information: DOI 10.1109/TPWRD.2020.2995879, IEEE Transactions on Power Delivery

[19] J. Turowski, M. Turowski and M. Kopec, "Method of three-dimensional network solution of leakage field of three-phase transformers," in IEEE Transactions on Magnetics, vol. 26, no. 5, pp. 2911-2919, Sept. 1990

[20] D. Dolinar, J. Pihler and B. Grcar, "Dynamic model of a three-phase power transformer," in IEEE Transactions on Power Delivery, vol. 8, no. 4, pp. 1811-1819, Oct. 1993

[21] B. A. Mork, F. Gonzalez, D. Ishchenko, D. L. Stuehm and J. Mitra, "Hybrid Transformer Model for Transient Simulation—Part I: Development and Parameters," in IEEE Transactions on Power Delivery, vol. 22, no. 1, pp. 248-255, Jan. 2007

[22] B. A. Mork, F. Gonzalez, D. Ishchenko, D. L. Stuehm and J. Mitra, "Hybrid Transformer Model for Transient Simulation—Part II: Laboratory Measurements and Benchmarking," in IEEE Transactions on Power Delivery, vol. 22, no. 1, pp. 256-262, Jan. 2007

[23] R. C. Degeneff, M. R. Gutierrez and P. J. McKenny, "A method for constructing a reduced order transformer model for system studies from detailed lumped parameter models," Proceedings of the 1991 IEEE Power Engineering Society Transmission and Distribution Conference, Dallas, TX, USA, 1991, pp. 532-538

[24] F. de Leon and A. Semlyen, "Reduced order model for transformer transients," in IEEE Transactions on Power Delivery, vol. 7, no. 1, pp. 361-369, Jan. 1992

[25] S. Okabe, M. Koto, G. Ueta, T. Saida and S. Yamada, "Development of high frequency circuit model for oil-immersed power transformers and its application for lightning surge analysis," in IEEE Transactions on Dielectrics and Electrical Insulation, vol. 18, no. 2, pp. 541-552, April 2011

[26] P. T. M. Vaessen, "Transformer model for high frequencies," in IEEE Transactions on Power Delivery, vol. 3, no. 4, pp. 1761-1768, Oct. 1988

[27] Q. Su, R. E. James and D. Sutanto, "A Z-transform model of transformers for the study of electromagnetic transients in power systems," in IEEE Transactions on Power Systems, vol. 5, no. 1, pp. 27-33, Feb. 1990

[28] A. Keyhani, S. W. Chua and S. A. Sebo, "Maximum likelihood estimation of transformer high frequency parameters from test data," in IEEE Transactions on Power Delivery, vol. 6, no. 2, pp. 858-865, April 1991

[29] A. Morched, L. Marti and J. Ottevangers, "A high frequency transformer model for the EMTP," in IEEE Transactions on Power Delivery, vol. 8, no. 3, pp. 1615-1626, July 1993

[30] Q. Wu, S. Jazebi and F. de Leon, "Parameter Estimation of Three-Phase Transformer Models for Low-Frequency Transient Studies from Terminal Measurements," in IEEE Transactions on Magnetics, vol. 53, no. 7, pp. 1-8, July 2017

[31] Q. Wu, T. Hong, S. Jazebi and F. de León, "Experimentally Validated Method to Measure the lambda–i Characteristics of Asymmetric Three-Phase Transformers," in IEEE Transactions on Magnetics, vol. 55, no. 4, pp. 1-9

[32] P. Vas, K. E. Hallenius, and J. E. Brown, "Cross-Saturation in Smooth-Air-Gap Electrical Machines," IEEE Transactions on Energy Conversion, vol. EC-1, no. 1, pp. 103–112, Mar. 1986

[33] L. Chedot and G. Friedrich, "A cross saturation model for interior permanent magnet synchronous machine. Application to a starter-generator," in Conference Record of the 2004 IEEE Industry Applications Conference, 2004. 39th IAS Annual Meeting., 2004, vol. 1, p. 70

[34] M. Dolinar, D. Dolinar, G. Stumberger, B. Polajzer and J. Ritonja, "A Three-Phase Core-Type Transformer Iron Core Model with Included Magnetic Cross Saturation," in IEEE Transactions on Magnetics, vol. 42, no. 10, pp. 2849-2851, Oct. 2006

[35] H. White, D. Woodson, "Electromechanical energy conversion," Wiley, 1959

[36] J. Meisel, "Principles of Electromechanical-Energy Conversion," McGraw-Hill, 1966

[37] A. Wilk, J. Nieznanski, I. Moson, P. Dobrowolski, and G. Kostro, "Nonlinear equivalent circuit model of a traction transformer for winding internal fault diagnostic purposes," in 2008 18th International Conference on Electrical Machines, 2008, pp. 1–5

[38] K. Umetani, "A generalized method for Lagrangian modeling of power conversion circuit with integrated magnetic components," IEEJ Transactions on Electrical and Electronic Engineering, vol. 7, no. S1, pp. S146–S152, 2012

[39] M. Noah, K. Umetani, J. Imaoka, and M. Yamamoto, "Lagrangian dynamics model and practical implementation of an integrated transformer in multi-phase LLC resonant converter," IET Power Electronics, vol. 11, no. 2, pp. 339–347, 2018

[40] T. Lagier et al., "A 100 kW 1.2 kV 20 kHz DC-DC converter prototype based on the Dual Active Bridge topology," 2018 IEEE International Conference on Industrial Technology (ICIT), Lyon, 2018, pp. 559-564

[41] P. Dworakowski, A. Wilk, M. Michna, B. Lefebvre and T. Lagier, "3-phase medium frequency transformer for a 100kW 1.2kV 20kHz Dual Active Bridge converter," IECON 2019 - 45th Annual Conference of the IEEE Industrial Electronics Society, Lisbon, Portugal, 2019, pp. 4071-4076

[42] G. Thaler, M. Wilcox, "Electric machines: dynamics and steady state," Wiley, 1966

[43] J. El Hayek and T. J. Sobczyk, "Equivalent circuit of multi-windings traction transformers including magnetizing currents," 2005 International Conference on Electrical Machines and Systems, Nanjing, 2005, pp. 1740-1745 Vol. 3

[44] E.F. Fuchs, Y. You, "Measurement of λ(i) characteristics of asymmetric three-phase transformers and their applications," Proceedings of the 9th International Conference on Harmonics and Quality Power, Orlando, Florida, USA, 1-4 October, 2000, pp.91-96

[45] P. Dworakowski, A. Wilk, M. Michna, B. Lefebvre, F. Sixdenier, and M. Mermet-Guyennet, "Effective Permeability of Multi Air Gap Ferrite Core 3-Phase Medium Frequency Transformer in Isolated DC-DC Converters," Energies, vol. 13, no. 6, p. 1352, Jan. 2020

[46] Ferroxcube, "3C90 material specification," Internet: https://www.ferroxcube.com/upload/media/product/file/MDS/3c90.pdf, Sep. 1, 2008, [Sep. 14, 2019]

[47] F. Tourkhani and P. Viarouge, "Accurate analytical model of winding losses in round Litz wire windings," in IEEE Transactions on Magnetics, vol. 37, no. 1, pp. 538-543, Jan 2001

[48] P. L. Dowell, "Effects of eddy currents in transformer windings," in Proceedings of the Institution of Electrical Engineers, vol. 113, no. 8, pp. 1387-1394, August 1966

[49] Wolfspeed, "CAS300M17BM2 1700V 225A 8.0mΩ SiC Half-Bridge." [Online]. Available: https://www.wolfspeed.com/power/products/sic-power-modules/cas300m17bm2. [Accessed: 01-Jan-2020]

[50] K. Venkatachalam, C. R. Sullivan, T. Abdallah and H. Tacca, "Accurate prediction of ferrite core loss with nonsinusoidal waveforms using only Steinmetz parameters," 2002 IEEE Workshop on Computers in Power Electronics, 2002. Proceedings., Mayaguez, Puerto Rico, USA, 2002, pp. 36-41

[51] C. P. Steinmetz, "On the Law of Hysteresis," in Transactions of the American Institute of Electrical Engineers, vol. IX, no. 1, pp. 1-64, Jan. 1892

Piotr Dworakowski received the M.Sc. degree in electrical engineering from Gdansk University of Technology, Poland, in 2007. Recently he has started the work towards the Ph.D. degree at the same university.

From 2008 to 2013 he was working with Alstom Transport, Tarbes, France on traction drives control. Since 2014 he has been a Power Converter Team Leader in SuperGrid Institute, Lyon, France. His research interests include high efficiency power converters for grids and transportation.

Andrzej Wilk (M'18) received the M.Sc., PhD, and D.Sc. ('habilitation') degrees in electrical engineering in 1983, 1995, and 2013, respectively, all from the Gdansk University of Technology (GUT), Poland.

He is with GUT since 1984, currently as an Associate Professor. His main scientific and research interests cover a wide spectrum of mathematical modeling and diagnosis of electromechanical converters using Lagrange's energetic approach and FEM-based computations. His research interests include transformers and electrical machines and diagnostics of railway trucks. He authored/co-authored more than 160 journal and conference papers.

Michal Michna (M'12-SM'18) received the M.Sc., Ph.D., degrees in electrical engineering in 1999 and 2005, respectively, all from Gdansk University of Technology (GUT), Poland.

He is with GUT since 1999, currently as an Assistant Professor. His main scientific and research interests cover a wide spectrum of mathematical modeling and diagnosis of electrical machines using analytical modeling and FEM-based computations.

Alexis Fouineau received the M.Sc. degree in electrical engineering from INSA de Lyon, France, in 2016, and the PhD degree in electrical engineering from Université Claude Bernard Lyon 1, France, in 2019.

Since 2019, he has been a research engineer in SuperGrid Institute, Lyon, France. His research interests are medium frequency transformers design and modeling, regarding both electromagnetic and thermal aspects.

Martin Guillet received the M.Sc. degree in general engineering from Ecole Centrale de Lyon, France, in 2006.

MOST WIEDZY Downloaded from mostwiedzy.pl

This work is licensed under a Creative Commons Attribution 4.0 License. For more information, see https://creativecommons.org/licenses/by/4.0/.

This article has been accepted for publication in a future issue of this journal, but has not been fully edited. Content may change prior to final publication. Citation information: DOI 10.1109/TPWRD.2020.2995879, IEEE Transactions on Power Delivery

From 2006 to 2017 he was working with Varioptic, Lyon, France on the design of optoelectronic components. Since 2017 he has been involved in the design of medium frequency transformers in SuperGrid Institute, Lyon, France.

MOST WIEDZY Downloaded from mostwiedzy.pl

This work is licensed under a Creative Commons Attribution 4.0 License. For more information, see https://creativecommons.org/licenses/by/4.0/.